Taylor & Francis
Taylor & Francis Group

Science and Technology of Advanced Materials: Methods

ISSN: 2766-0400 (Online) Journal homepage: www.tandfonline.com/journals/tstm20

Ultrathin photonic–plasmonic membranes supporting high-Q hybrid bound states in the continuum

Ya-Lun Ho, Mu-Hsin Chen, Chih-Zong Deng, Chun-Hao Chiang, Hsin-Chang Lin, Yen-Ju Wu & Masanobu Iwanaga

To cite this article: Ya-Lun Ho, Mu-Hsin Chen, Chih-Zong Deng, Chun-Hao Chiang, Hsin-Chang Lin, Yen-Ju Wu & Masanobu Iwanaga (2026) Ultrathin photonic–plasmonic membranes supporting high-Q hybrid bound states in the continuum, Science and Technology of Advanced Materials: Methods, 6:1, 2639793, DOI: 10.1080/27660400.2026.2639793

To link to this article: https://doi.org/10.1080/27660400.2026.2639793

Published online: 17 Mar 2026.

SCIENCE AND TECHNOLOGY OF ADVANCED MATERIALS: METHODS
2026, VOL. 6, NO. 1, 2639793
https://doi.org/10.1080/27660400.2026.2639793

Ultrathin photonic–plasmonic membranes supporting high-Q hybrid bound states in the continuum

Ya-Lun Ho [a], Mu-Hsin Chen [a], Chih-Zong Deng [a], Chun-Hao Chiang [a], Hsin-Chang Lin [b], Yen-Ju Wu [c] and Masanobu Iwanaga [a]

[a]Research Center for Electronic and Optical Materials, National Institute for Materials Science (NIMS), Tsukuba, Japan; [b]Department of Electronic and Computer Engineering, National Taiwan University of Science and Technology, Taipei, Taiwan; [c]Center for Basic Research on Materials, National Institute for Materials Science (NIMS), Tsukuba, Japan

ABSTRACT

Plasmonic bound states in the continuum (BICs) offer a promising route to overcome the intrinsic trade-off between field confinement and radiation loss in nanophotonic systems. By exploiting the coupling of plasmonic and photonic systems, plasmonic BICs can achieve sharp spectral selectivity with strong near-field enhancement, making them attractive for compact and efficient optical devices. However, realizing high-Q resonances in plasmonic structures remains challenging due to Ohmic losses and the requirement of relatively thick metallic films. Here, we numerically demonstrate an ultrathin freestanding photonic – plasmonic membrane that supports hybrid guided and quasi-BIC resonances with record-high Q-factors in plasmonic architectures. By integrating a thin Ag layer (10–20 nm) with a dielectric SiN membrane, the hybrid coupling suppresses radiative leakage while preserving deep-subwavelength confinement, yielding Q-factors exceeding 2370. Remarkably, even when the total thickness of the photonic-plasmonic membrane is reduced to approximately 30 nm, the resonance maintains $Q > 1300$ with strong near-field intensity, a performance regime that cannot be achieved in metal-only plasmonic systems. The demonstrated strategy resolves the long-standing trade-off between near-field localization and radiative loss in plasmonics by leveraging hybrid BIC formation in an ultrathin membrane platform. Because the architecture is compatible with standard thin-film processing and operates with metal layers only a few tens of nanometers thick, it provides a practical route to compact, high-performance components for nanophotonic sensing, surface-enhanced spectroscopy, quantum emitter coupling, nonlinear optics, and subwavelength optoelectronics.

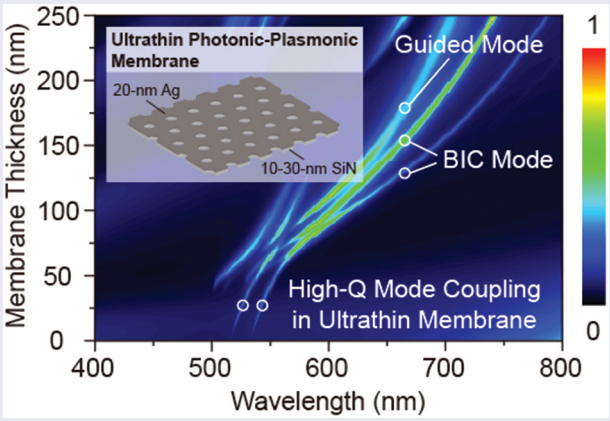

IMPACT STATEMENT

Ultrathin photonic–plasmonic membranes support high-Q (>2000) hybrid bound states in the continuum, overcoming plasmonic limitations and enabling strong light confinement in subwavelength architectures for compact nanophotonic devices.

ARTICLE HISTORY
Received 9 November 2025
Revised 27 January 2026
Accepted 27 February 2026

KEYWORDS
Plasmonic; photonic–plasmonic hybrid BICs; bound states in the continuum (BICs); high-Q; ultrathin metasurface; nanomembrane

1. Introduction

Controlling radiative losses in nanophotonic systems has become a key strategy for engineering high-Q resonances to enhance light – matter interactions at the nanoscale. Bound states in the continuum (BICs) [1–5] have emerged as a promising candidate to achieve this goal by suppressing radiation despite being embedded in the continuum of free-space modes. By leveraging the physics of BICs, dielectric

CONTACT Ya-Lun Ho HO.Ya-Lun@nims.go.jp Research Center for Electronic and Optical Materials, National Institute for Materials Science (NIMS), 1-1 Namiki, Tsukuba, Ibaraki 305-0044, Japan

metasurfaces and photonic crystal slabs have been widely exploited to realize high-Q resonances, enabling diverse applications ranging from low-threshold lasing and ultrasensitive biosensing to nonlinear optics [6–12]. However, despite their superior spectral selectivity, these dielectric systems are fundamentally limited by large mode volumes. This restricts strong field confinement and thus limits the coupling efficiency with subwavelength active materials, such as quantum emitters, molecular monolayers, and two-dimensional materials.

Plasmonic structures, supporting surface plasmon resonances at the metallic surface, offer strong near-field enhancement and deep subwavelength confinement [13–16]. However, their performance is often hindered by intrinsic Ohmic losses, limiting Q-factors and spectral selectivity. The concept of plasmonic BICs, emerging from designs such as metallic nanoparticle arrays [16–18], mirror-coupled plasmonic resonators [19], metal-insulator-metal (MIM) metasurfaces [20–22], and chiral plasmonic metasurfaces [23], seeks to bridge these limitations by introducing symmetry-protected or interference-based suppression of radiative losses within plasmonic architectures.

Furthermore, the incorporation of metallic components in BIC structures introduces distinct advantages for practical applications. The strong field confinement and formation of nanoscale hotspots around metal interfaces enable enhanced light – matter coupling far beyond what purely dielectric BICs can offer. This advantage has been demonstrated across several key areas. In biosensing, plasmonic BICs achieve ultrahigh molecular sensitivity due to increased overlaps between the localized field and the analyte region [24,25]. In sub-bandgap photodetection, metal-based BICs enable efficient hot-carrier generation through nonradiative plasmon decay, a mechanism absent in dielectric systems [22]. In nonlinear optics and surface-enhanced Raman scattering, the near-field amplification associated with plasmonic BICs significantly boosts conversion efficiencies and detection limits [24–27]. Collectively, these results highlight that metallic elements are not merely structural modifiers but are essential for achieving functionalities unattainable with dielectric BICs alone.

Recent studies have demonstrated plasmonic BICs with improved Q-factors while maintaining ultra-small effective mode volumes, leading to advances in applications such as hot-electron photodetection [22], perfect absorption [19], nonlinear harmonic generation [21], biosensing [24,25], and lasing [23,28]. Hybrid photonic – plasmonic designs that couple plasmonic structures with dielectric resonators further decrease mode volumes, enabling more efficient light – matter coupling. For example, hybrid photonic – plasmonic BIC systems leveraging out-of-plane symmetry breaking in metasurface geometries [18], hybrid MIM-dielectric architectures [22], and topologically protected hybrid systems [21] have been shown to achieve tunable, high-Q modes with strong field localization. While plasmonic BICs have opened new opportunities for manipulating light – matter interactions at the nanoscale, realizing high-Q resonances with strong confinement remains difficult due to metallic absorption losses and structural complexity [20,29]. These challenges motivate the exploration of ultrathin or hybrid photonic – plasmonic systems [25,30,31] that can retain high Q-factors while achieving deep subwavelength field confinement.

In this work, we numerically demonstrate an ultrathin freestanding photonic – plasmonic membrane that supports hybrid guided modes (GMs) and quasi-BIC modes, enabling high-Q resonances through metal – dielectric coupling. The ultrathin form factor of membrane-based nanophotonic architectures provides unique advantages for integration into compact optical systems. Such freestanding architectures have been successfully demonstrated in ultrafast all-optical switching and chiral metasurface platforms [32,33], highlighting their potential for advanced light manipulation. The proposed structure integrates a thin plasmonic metal layer (10–20 nm) with a photonic membrane [34–39], forming a strongly confined hybrid mode where the photonic and plasmonic fields interact constructively to suppress radiative leakage. When the metallic layer thickness is optimized, the hybrid photonic – plasmonic quasi-BIC exhibits a Q-factor approaching 2370, which is among the highest values reported for plasmonic BIC structures. Furthermore, reducing the dielectric thickness down to 20 nm sustains the high-Q resonance while simultaneously enhancing the field confinement. These findings demonstrate that high-Q plasmonic resonances can be achieved in a deeply subwavelength membrane structure via hybrid quasi-BIC coupling between ultrathin metal and dielectric layers. The resulting configuration, consisting of a 20-nm dielectric slab combined with an equally thin metal film, yields a strongly confined, low-radiation-loss mode that cannot be achieved with conventional metal-only plasmonic systems. This work highlights the potential of hybrid BIC strategies based on the photonic-plasmonic membrane that combine the low-loss nature of dielectric resonators with the extreme near-field enhancement of plasmonic modes, offering new opportunities for compact and high-performance platforms in nanophotonics, quantum photonics, optoelectronics, nonlinear optics, and biosensing.

2. Results and discussions

Figure 1(a) shows the schematic illustration of the proposed photonic – plasmonic membrane structure, consisting of a dielectric (SiN) slab with a triangular lattice of air holes and a thin metal (Ag) layer deposited on top. The membrane geometry is defined by the lattice period (P), hole radius (R), dielectric slab thickness (T_{SiN}), and metal layer thickness (T_{Ag}). The simulations were performed using rigorous coupled-wave analysis (DiffractMOD, RSoft Design Group, U.S.A.) under periodic boundary conditions in the x- and y-axes and perfectly-matched-layer conditions in the z-axis for an air-suspended photonic membrane ($T_{Ag} = 0$) with parameters $p = 600$ nm, $R = 150$ nm, and $T_{SiN} = 150$ nm, representing the dielectric structure without the metal

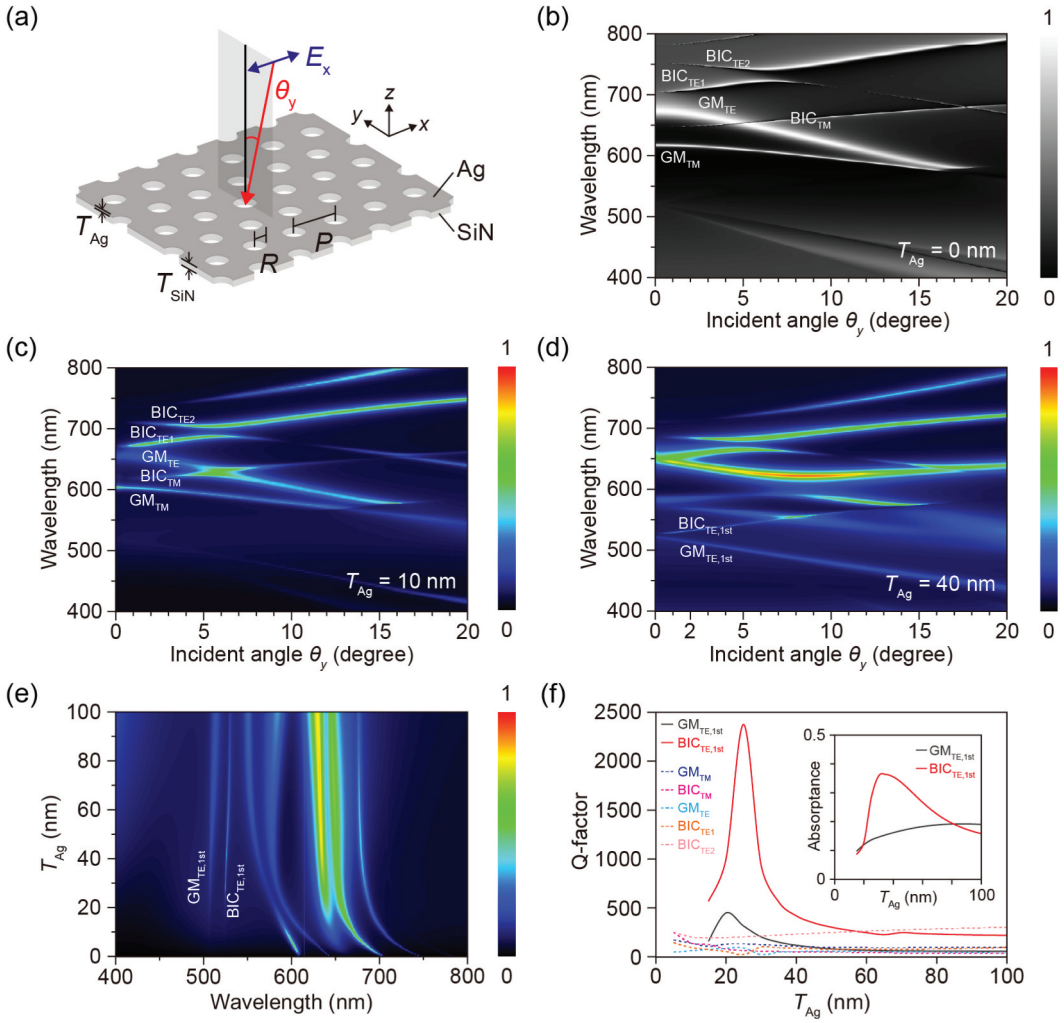

Figure 1. (a) Schematic diagram of the photonic – plasmonic membrane supporting high-Q hybrid quasi-BICs. The membrane consists of a triangular lattice of air holes with a lattice period $p = 600$ nm and radius $R = 150$ nm in a dielectric (SiN) slab of thickness $T_{SiN} = 150$ nm, integrated with a plasmonic metal (Ag) layer of variable thickness (T_{Ag}) on the top surface. The schematic also illustrates the incident light angle along the y-axis (θ_y) and polarization along the x-direction (E_x). (b) Simulated reflectance spectra as a function of θ_y for the photonic membrane without a metal layer. (c,d) Simulated absorptance spectra as functions of θ_y for the plasmonic – photonic membrane with T_{Ag} = (c) 10 nm and (d) 40 nm, respectively. (e) Simulated absorptance spectra as a function of T_{Ag} for the plasmonic – photonic membrane at $\theta_y = 2°$. (f) Simulated variation of the resonance-mode Q factor as a function of T_{Ag}. Inset: absorptance variation of the higher-order GM and BIC indicated in (f).

film, as shown in Figure 1(b). The optical properties of SiN and Ag were taken from the previous studies [40,41]. The angle-dependent reflectance spectra were calculated for x-polarized excitation under varying incident angles (θ_y) along the y-axis, ranging from 0° to 20°, to investigate symmetry-protected BICs near the Γ point. Two resonances appear near 615 nm and 668 nm at normal incidence, corresponding to guided modes GM_{TM} and GM_{TE}, respectively. The transverse electric (TE) and transverse magnetic (TM) characteristics of these modes were identified through the field component distributions. In contrast, additional narrow resonances observed around 640–710 nm are attributed to quasi-BIC modes (BIC_{TM}, BIC_{TE1}, and BIC_{TE2}), exhibiting vanishing radiative intensity at 0° and extremely narrow linewidths. While the guided modes maintain relatively broad bandwidths, the quasi-BIC resonances display linewidths approaching zero as the incidence angle approaches normal.

After investigating the photonic membrane supporting both guided and quasi-BIC modes, we next examined the influence of plasmonic effects by introducing a metal layer on top, forming a plasmonic – photonic membrane structure. Figure 1(c,d) present the simulated dispersion diagrams of the same structure as in Figure 1(b), but with Ag layers of 10-nm and 40-nm thickness, respectively. Due to the intrinsic Ohmic loss of Ag, absorptance was calculated and used to construct the dispersion diagrams for clearer visualization of resonant features. Compared with the photonic membrane (Figure 1(b)), the structure with a 10-nm Ag layer (Figure 1(c)) exhibits a similar dispersion relation. However, the resonance linewidths, particularly that of the quasi-BIC resonance, become noticeably

broader, indicating the effect of increased metallic loss. In Figure 1(d), when the metal thickness increases to 40 nm, two additional split resonances appear near 520 nm at small incident angles, which are not present in Figure 1(b,c). These two modes, denoted as $GM_{TE,1st}$ and $BIC_{TE,1st}$, correspond to higher-order resonances supported by the photonic – plasmonic membrane once the metal layer reaches a certain critical thickness. With further increase in Ag thickness, both modes broaden and their absorptance gradually decreases. Figure 1(e) shows the spectral variation as a function of Ag thickness at an incident angle of 2°, clearly illustrating the evolution of resonance modes. The extracted Q-factor variations from these spectra are plotted in Figure 1(f). $GM_{TE,1st}$ and $BIC_{TE,1st}$ show distinct behavior. Rather than evolving continuously from the photonic case ($T_{Ag} = 0$), they reach their maximum Q-factors of approximately 450 and 2370 at $T_{Ag} = 20$ and 25 nm, respectively. Notably, $BIC_{TE,1st}$ achieves maximum absorptance at $T_{Ag} \approx 25$ nm, indicating the optimized hybrid coupling condition.

To further clarify the correspondence between the resonance modes in the photonic and photonic – plasmonic membranes, we analyzed the near-field distributions, represented by the electric energy density at the metal – dielectric interface in the xy plane. The electric energy density is defined as $U_E = \frac{1}{2}\int \mathrm{Re}[\varepsilon(\mathbf{r}')]|E|^2\, dV$, where E is the electric field normalized by the amplitude of the incident light, ε is the spatially dependent permittivity, and V is the volume of the simulation grid. Figure 2(a,c) show the calculated reflectance and absorptance spectra for the photonic membrane and the photonic – plasmonic membrane, respectively. The spectra at incident angles of 0° and 2° are chosen to distinguish between the GMs and BICs. For the photonic membrane, the resonance at 615 nm corresponds to GM_{TM}, exhibiting strong field enhancement between air holes along the x-direction, as shown in Figure 2(b). The narrow resonance at 648 nm shows field localization between holes along the y-direction, corresponding to BIC_{TM}. The mode at 668 nm displays a broader spectral response with the field concentrated inside the air holes rather than within the dielectric, corresponding to GM_{TE}. BIC_{TE1} appears at 707 nm with strong energy density localized at the hole edges, while another mode, BIC_{TE2}, emerges at 748 nm with the field predominantly oriented along the x-direction. For the plasmonic – photonic membrane, GMs and BICs exhibit spatial distributions similar to their photonic counterparts, as shown in Figure 2(d), indicating the hybridized nature of the hybrid plasmonic – photonic modes. It is noted that two resonances at 586 nm and 598 nm (CM_1 and CM_2) display coupling between GM and BIC modes, consistent with the mode interaction seen in Figure 1(d). Furthermore, two additional higher-order modes, $GM_{TE,1st}$ and $BIC_{TE,1st}$, as indicated in Figure 1(d,e), appear at 510 nm and 528 nm, respectively. These modes, characterized by narrow linewidths, are unique to the plasmonic – photonic membrane and are absent in the purely photonic case.

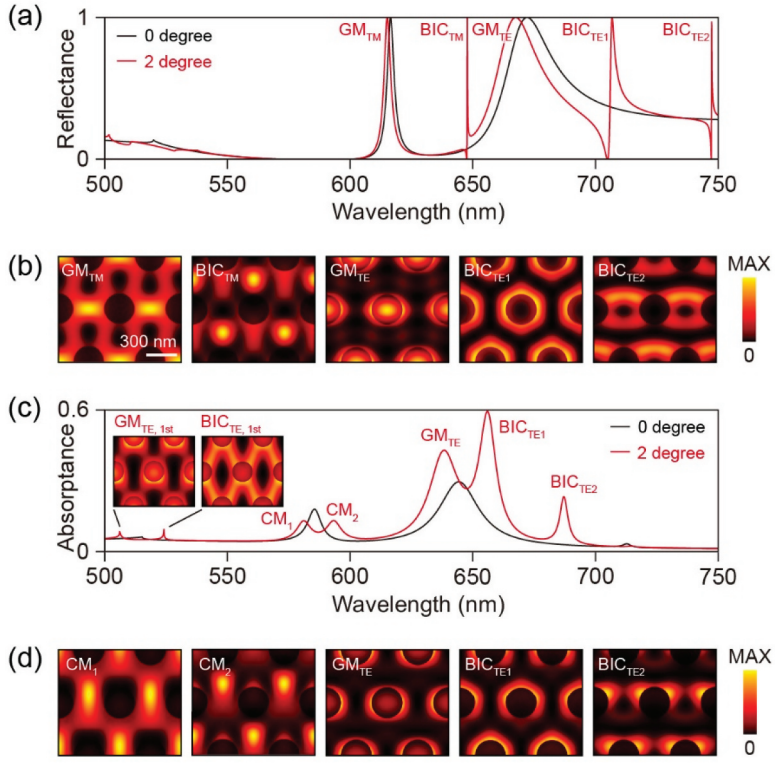

Figure 2. (a,c) Simulated reflectance/absorptance spectra of (a) the photonic membrane and (c) the photonic – plasmonic membrane (T_{Ag} = 20 nm) at $\theta_y = 0°$ (black) and $\theta_y = 2°$ (red). (b) Electric energy density distributions of the GMs and BICs observed in the photonic membrane. The distributions are taken on the xy plane at the SiN – air interface under illumination. (d) Electric energy density distributions of the hybrid modes observed in the photonic – plasmonic membrane. The distributions are taken on the xy plane at the SiN–Ag interface.

To investigate the influence of the dielectric slab thickness on the coupling between surface plasmon and photonic modes, we calculated the resonance spectra as a function of dielectric thickness. Figures 3(a,b) show the reflectance spectra of the photonic membrane and the absorptance spectra of the plasmonic – photonic membrane with a 20-nm Ag layer, respectively, at the incident angle of 2°. In the photonic case, both guided and quasi-BIC modes exhibit a continuous blueshift as the dielectric membrane becomes thinner, maintaining smooth resonance evolution without pronounced mode coupling, except where two guided modes merge near $T_{SiN} = 230$ nm. In contrast, the plasmonic – photonic membrane displays markedly different behavior. For dielectric thicknesses above 100 nm, the guided and quasi-BIC modes remain distinct. However, as the thickness decreases below 100 nm, these resonances merge and undergo abrupt spectral transitions. Figure 3(c) presents the spatial electric energy distributions of the resonances indicated in Figure 3(b), confirming that their near-field profiles correspond to those observed in Figure 2(d). When the dielectric thickness is reduced below 40 nm, only two resonant modes remain. These modes exhibit narrow linewidths and significantly enhanced intensity compared with higher-order GMs and BICs at similar wavelengths in thicker membranes, demonstrating the formation of strongly confined hybrid modes in the ultrathin photonic – plasmonic membrane.

Figure 3(d) shows the dispersion diagram of the photonic – plasmonic membrane composed of a 20-nm SiN layer and a 20-nm Ag layer, where GM and quasi-BIC resonances appear near normal incidence with mode coupling. In Figure 3(e), the corresponding electric energy distributions reveal fields strongly localized near the air holes and extending along the *y*-direction. The electric field amplitude and

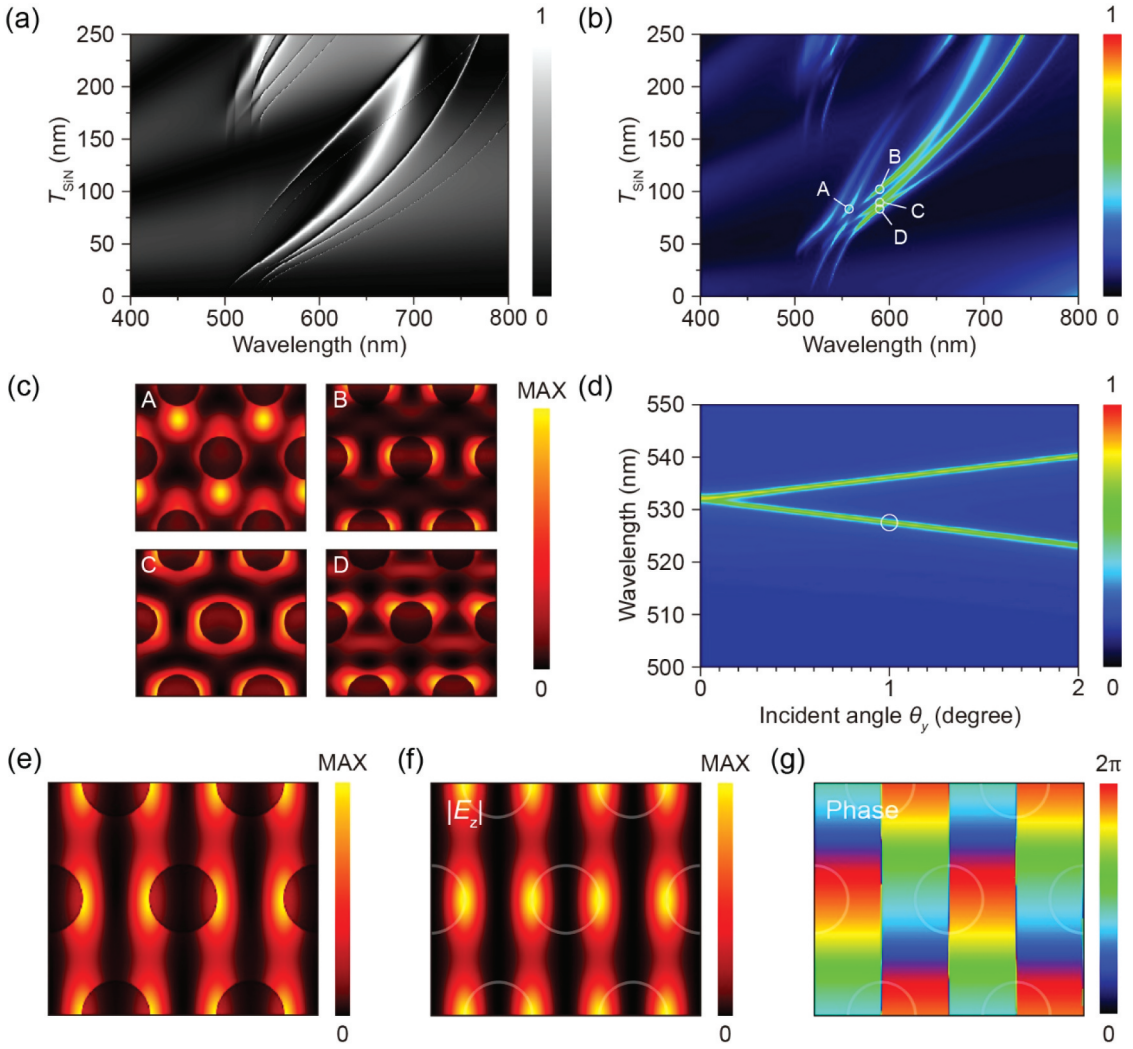

Figure 3. (a) Simulated reflectance spectra as a function of T_{SiN} for the photonic membrane at $\theta_y = 2°$. (b) Simulated absorptance spectra as a function of T_{SiN} for the photonic – plasmonic membrane with $T_{Ag} = 20$ nm at $\theta_y = 2°$. (c) Electric energy density distributions of the hybrid GM and BICs indicated in (b). The distributions are taken on the xy plane at the SiN–Ag interface. (d) Simulated absorptance spectra as a function of θ_y for the ultrathin photonic – plasmonic membrane ($T_{SiN} = 20$ nm, $T_{Ag} = 20$ nm). (e) Electric energy density distribution and the dominant out-of-plane electric-field (E_z) (f) amplitude and (g) phase distributions of the hybrid quasi-BIC indicated in (d). The distributions are taken on the xy plane at the SiN–Ag interface.

phase distributions of the dominant out-of-plane E_z component (Figure 3(e–g)) at the resonance marked in Figure 3 (d) confirm the anti-symmetric distribution characteristic of the hybrid photonic – plasmonic quasi-BICs.

From the results in Figure 3, it can be concluded that narrowband hybrid photonic – plasmonic modes can be achieved by coupling ultrathin dielectric membranes with thin metallic layers. To further compare these hybrid photonic – plasmonic modes with pure plasmonic resonances, we simulated a reference structure consisting solely of a metal hole-array membrane without any dielectric component. Figure 4(a,b) show the absorptance spectra as a function of Ag thickness for the photonic – plasmonic membrane (with a 20-nm SiN layer) and the pure plasmonic membrane, respectively. In the photonic – plasmonic membrane, narrowband resonances appear even when the Ag layer is thinner than 20 nm, whereas in the pure plasmonic membrane, resonances emerge only when the Ag thickness exceeds 50 nm. Furthermore, the resonance intensity in the photonic – plasmonic membrane is substantially stronger than that in the metal-only counterpart. For the hybrid quasi-BIC mode, the Q-factor reaches approximately 1380 when the Ag thickness is 10 nm. Figure 4(c) compares the absorptance spectra of the photonic – plasmonic membrane (20-nm SiN/20-nm Ag) and the pure plasmonic membrane (40-nm Ag), together with their corresponding absorption distributions at the metal surface under normal incidence. The hybrid photonic – plasmonic membrane exhibits a maximum absorption intensity approximately five times higher than that of the pure plasmonic case, confirming the superior field confinement and energy localization enabled by hybrid quasi-BIC formation. Synthesizing the analysis of structural variations presented above, two distinct design regimes were identified for the proposed photonic – plasmonic membrane. The thicker dielectric configuration (T_{SiN} = 150 nm) supports the highest Q-factor (~2370), representing the design for applications prioritizing maximum spectral selectivity. In contrast, the ultrathin configuration (T_{SiN} = 20 nm, T_{Ag} = 20 nm) demonstrates the hybrid architecture's capability to maintain a high Q-factor (~1380) and strong absorption even at the limit of physical thickness. This latter regime is particularly significant for developing extremely compact, flexible nanophotonic devices where minimizing the device footprint and mode volume is the primary design criterion. Furthermore, it is noted that while Ag was selected for this study due to its minimal ohmic losses in the visible spectrum, which is critical for achieving the highest possible Q-factors, its chemical stability is a known concern. Alternative plasmonic materials such as Au or Al offer

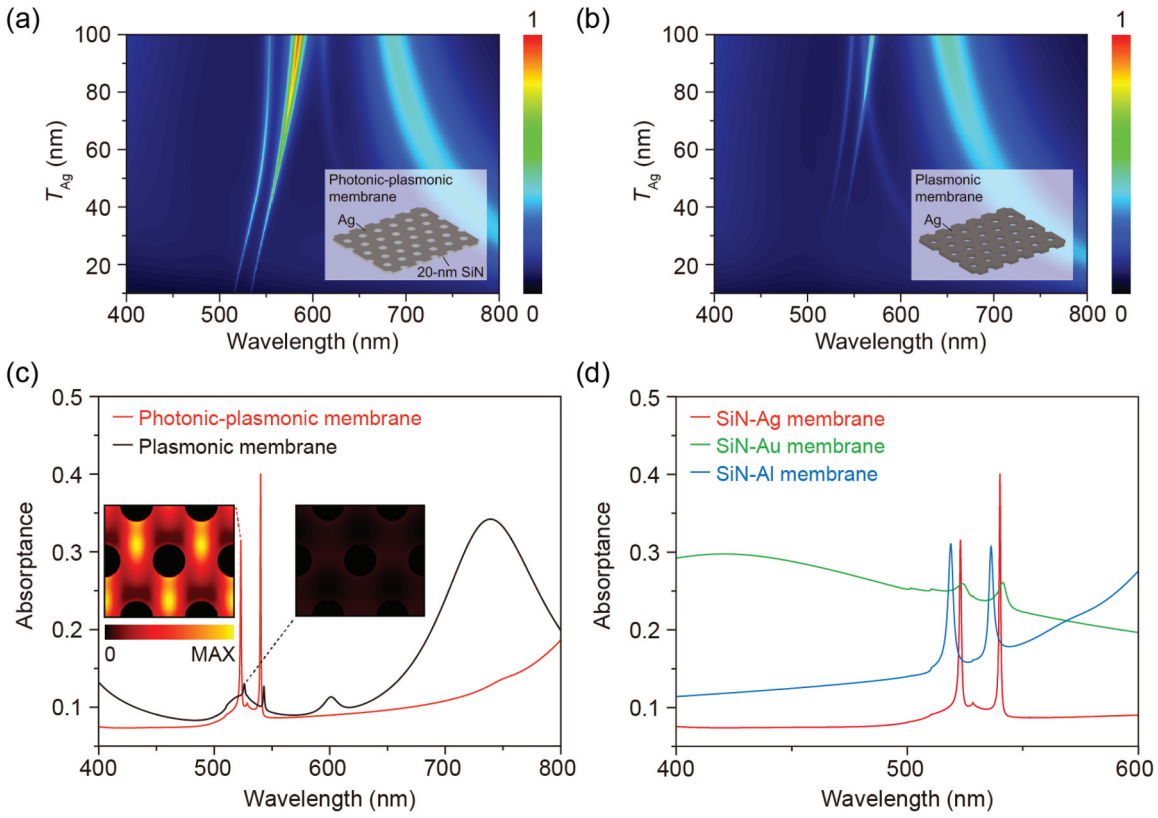

Figure 4. (a) Simulated absorptance spectra as a function of T_{Ag} for the photonic – plasmonic membrane with T_{SiN} = 20 nm at θ_y = 2°. (b) Simulated absorptance spectra as a function of metal layer thickness (T_{Ag}) for the pure plasmonic membrane (metal-only structure). (c) Simulated absorptance spectra of the photonic – plasmonic membrane (T_{SiN} = 20 nm, T_{Ag} = 20 nm) and the pure plasmonic membrane (T_{Ag} = 40 nm) at θ_y = 2°. Insets: absorption distributions of the hybrid quasi-BIC and pure plasmonic quasi-BIC modes indicated in (c), taken on the xy plane at the Ag – air interface. (d) Comparison of simulated absorptance spectra for the photonic – plasmonic membrane (T_{SiN} = 20 nm) with Ag, Au, and Al layers of the same thickness (20 nm) at θ_y = 2°.

superior environmental stability; however, our preliminary simulations suggest that substituting Ag with Au or Al would lead to increased damping and broader resonance linewidths, thereby reducing the Q-factor and the absorptance of the hybrid BIC modes, as shown in Figure 4(d). For practical applications requiring long-term durability, a thin protective passivation dielectric layer on the Ag surface or the use of Au could be considered, though with a trade-off in the sharpness of the resonance.

It is worth noting that the sharp absorption features observed in our hybrid system arise from the critical coupling between the incident light and the quasi-BIC mode. As the radiative loss channel is suppressed near the BIC condition, it can be matched with the intrinsic non-radiative loss (ohmic loss) of the metal, resulting in strong and high-Q absorption. This sharp spectral feature is phenomenologically similar to electromagnetically induced absorption [42], where destructive interference suppresses the reflection, channeling energy into absorption [43]. Unlike conventional broadband plasmonic absorbers, our hybrid architecture enables narrowband absorption, which is advantageous for sensing and filtering applications.

3. Conclusions

In summary, we have designed and analyzed a plasmon-coupled photonic membrane that simultaneously supports GM and quasi-BIC resonances. By integrating an ultrathin metallic layer (10–20 nm thick) with a dielectric membrane, narrowband resonances with significantly enhanced intensity are achieved. Such performance cannot be realized in conventional metal-only plasmonic systems. In addition to its superior optical characteristics, the proposed architecture is compatible with standard nanofabrication processes and provides greater structural flexibility than pure metal membranes. The demonstrated photonic – plasmonic membrane supporting narrowband quasi-BIC modes thus represents a promising platform for high-sensitivity biosensing, surface-enhanced Raman scattering, photodetection, and photocatalysis, where both strong field localization and sharp spectral selectivity are essential.

Disclosure statement

No potential conflict of interest was reported by the author(s).

Funding

The work was supported by the JSPS KAKENHI Grant Number [JP23K26155 and JP25KF0083].

ORCID

Ya-Lun Ho http://orcid.org/0000-0001-8274-5978
Mu-Hsin Chen http://orcid.org/0000-0002-3885-5720
Chih-Zong Deng http://orcid.org/0009-0005-2398-5353
Chun-Hao Chiang http://orcid.org/0000-0002-9066-4657
Hsin-Chang Lin http://orcid.org/0000-0001-8384-6690
Yen-Ju Wu http://orcid.org/0000-0003-2647-3407
Masanobu Iwanaga http://orcid.org/0000-0002-8930-6940

Data availability statement

The data that support the findings of this study are available from the corresponding author upon reasonable request.

References

[1] Marinica DC, Borisov AG, Shabanov SV. Bound states in the continuum in photonics. Phys Rev Lett. 2008;100(18):183902. doi: 10.1103/PhysRevLett.100.183902
[2] Yang Y, Peng C, Liang Y, et al. Analytical perspective for bound states in the continuum in photonic crystal slabs. Phys Rev Lett. 2014;113(3):037401. doi: 10.1103/PhysRevLett.113.037401
[3] Hsu CW, Zhen B, Stone AD, et al. Bound states in the continuum. Nat Rev Mater. 2016;1(9):16048. doi: 10.1038/natrevmats.2016.48
[4] Joseph S, Pandey S, Sarkar S, et al. Bound states in the continuum in resonant nanostructures: an overview of engineered materials for tailored applications. Nanophotonics. 2021;10(17):4175–4207. doi: 10.1515/nanoph-2021-0387
[5] Yang J-H, Huang Z-T, Maksimov DN, et al. Low-threshold bound state in the continuum lasers in hybrid lattice resonance metasurfaces. Laser Photonics Rev. 2021;15(10):2100118. doi: 10.1002/lpor.202100118
[6] Richter FU, Sinev I, Zhou S, et al. Gradient high-Q dielectric metasurfaces for broadband sensing and control of vibrational light-matter coupling. Adv Mater. 2024;36(25):2314279. doi: 10.1002/adma.202314279
[7] Sinev IS, Koshelev K, Liu Z, et al. Observation of ultrafast self-action effects in quasi-BIC resonant metasurfaces. Nano Lett. 2021;21(20):8848–8855. doi: 10.1021/acs.nanolett.1c03257
[8] Hsiao H-H, Hsieh J-C, Liu A-Y, et al. Enhancement of third-harmonic generation in all-dielectric kite-shaped metasurfaces driven by quasi-bound states in the continuum. Nanophotonics. 2024;13(17):3155–3164. doi: 10.1515/nanoph-2024-0194
[9] Liu A-Y, Lin K-I, Tseng SH, et al. Broadband enhancement of third harmonic generation based on the strong coupling between all-dielectric metasurfaces and epsilon-near-zero modes. Adv Opt Mater. 2025;13(19):2500084. doi: 10.1002/adom.202500084
[10] Hwang M-S, Lee H-C, Kim K-H, et al. Ultralow-threshold laser using super-bound states in the continuum. Nat Commun. 2021;12(1):4135. doi: 10.1038/s41467-021-24502-0
[11] Jahani Y, Arvelo ER, Yesilkoy F, et al. Imaging-based spectrometer-less optofluidic biosensors based on dielectric metasurfaces for detecting extracellular vesicles. Nat Commun. 2021;12(1):3246. doi: 10.1038/s41467-021-23257-y

[12] Zograf G, Koshelev K, Zalogina A, et al. High-harmonic generation from resonant dielectric metasurfaces empowered by bound states in the continuum. ACS Photonics. 2022;9(2):567–574. doi: 10.1021/acsphotonics.1c01511
[13] Seo IC, Kim S, Woo BH, et al. Fourier-plane investigation of plasmonic bound states in the continuum and molecular emission coupling. Nanophotonics. 2020;9(15):4565–4577. doi: 10.1515/nanoph-2020-0343
[14] Wang Z, Wang Y, Cheng Z, et al. Tunable flatband plasmonic quasi-bound states in the continuum based on graphene-assisted metasurfaces. Appl Phys Lett. 2023;123(12). doi: 10.1063/5.0166140
[15] Liang Y, Koshelev K, Zhang F, et al. Bound states in the continuum in anisotropic plasmonic metasurfaces. Nano Lett. 2020;20(9):6351–6356. doi: 10.1021/acs.nanolett.0c01752
[16] Wang Z, Li L, Shi X, et al. Bound states in the continuum induced by the strong coupling within the plasmonic lattices. J Appl Phys. 2023;133(15). doi: 10.1063/5.0148144
[17] Aigner A, Tittl A, Wang J, et al. Plasmonic bound states in the continuum to tailor light-matter coupling. Sci Adv. 2022;8(49):eadd4816. doi: 10.1126/sciadv.add4816
[18] Liang Y, Tsai DP, Kivshar Y. From local to nonlocal high-Q plasmonic metasurfaces. Phys Rev Lett. 2024;133(5):053801. doi: 10.1103/PhysRevLett.133.053801
[19] Wang J, Weber T, Aigner A, et al. Mirror-coupled plasmonic bound states in the continuum for tunable perfect absorption. Laser Photonics Rev. 2023;17(11):2300294. doi: 10.1002/lpor.202300294
[20] Cao F, Zhou M, Cheng C-W, et al. Interaction of plasmonic bound states in the continuum. Photon Res. 2023;11(5):724–731. doi: 10.1364/PRJ.480968
[21] Shen S, Liu W, He J, et al. Topologically protected plasmonic bound states in the continuum. Nano Lett. 2024;24(42):13285–13292. doi: 10.1021/acs.nanolett.4c03636
[22] Wang Z, Sun J, Wu C, et al. Plasmonic bound states in the continuum metasurface–semiconductor–metal architecture enables efficient hot-electron-based photodetector. ACS Appl Mater Interface. 2024;16(25):32836–32846. doi: 10.1021/acsami.4c03770
[23] Tang Y, Liang Y, Yao J, et al. Chiral bound states in the continuum in plasmonic metasurfaces. Laser Photonics Rev. 2023;17(4):2200597. doi: 10.1002/lpor.202200597
[24] Clabassi E, Balestra G, Siciliano G, et al. Hybrid plasmonic symmetry-protected bound state in the continuum entering the zeptomolar biodetection range. Small. 2025;21(10):2411827. doi: 10.1002/smll.202411827
[25] Luo M, Zhou Y, Zhao X, et al. High-sensitivity optical sensors empowered by quasi-bound states in the continuum in a hybrid metal–dielectric metasurface. ACS Nano. 2024;18(8):6477–6486. doi: 10.1021/acsnano.3c11994
[26] Zhou Y, Guo Z, Zhao X, et al. Dual-quasi bound states in the continuum enabled plasmonic metasurfaces. Adv Opt Mater. 2022;10(19):2200965. doi: 10.1002/adom.202200965
[27] Zheng M, Shen Y, Zou Q, et al. Moisture-driven switching of plasmonic bound states in the continuum in the visible region. Adv Funct Mater. 2023;33(3):2209368. doi: 10.1002/adfm.202209368
[28] Heilmann R, Salerno G, Cuerda J, et al. Quasi-BIC mode lasing in a quadrumer plasmonic lattice. ACS Photonics. 2022;9(1):224–232. doi: 10.1021/acsphotonics.1c01416
[29] Wang Z, Liang Y, Qu J, et al. Plasmonic bound states in the continuum for unpolarized weak spatially coherent light. Photon Res. 2023;11(2):260–269. doi: 10.1364/PRJ.477385
[30] Joseph S, Sarkar S, Khan S, et al. Exploring the optical bound state in the continuum in a dielectric grating coupled plasmonic hybrid system. Adv Opt Mater. 2021;9(8):2001895. doi: 10.1002/adom.202001895
[31] Meudt M, Bogiadzi C, Wrobel K, et al. Hybrid photonic–plasmonic bound states in continuum for enhanced light manipulation. Adv Opt Mater. 2020;8(20):2000898. doi: 10.1002/adom.202000898
[32] Tseng ML, Lin Z-H, Kuo HY, et al. Stress-induced 3d chiral fractal metasurface for enhanced and stabilized broadband near-field optical chirality. Adv Opt Mater. 2019;7(15):1900617. doi: 10.1002/adom.201900617
[33] Fang X, Lun Tseng M, Ou J-Y, et al. Ultrafast all-optical switching via coherent modulation of metamaterial absorption. Appl Phys Lett. 2014;104(14):141102. doi: 10.1063/1.4870635
[34] Rosas S, Adi W, Beisenova A, et al. Enhanced biochemical sensing with high-Q transmission resonances in free-standing membrane metasurfaces. Optica. 2025;12(2):178–189. doi: 10.1364/OPTICA.549393
[35] Ma X, Kudtarkar K, Chen Y, et al. Coherent momentum control of forbidden excitons. Nat Commun. 2022;13(1):6916. doi: 10.1038/s41467-022-34740-5
[36] Ho Y-L, Fong CF, Wu Y-J, et al. Finite-area membrane metasurfaces for enhancing light-matter coupling in monolayer transition metal dichalcogenides. ACS Nano. 2024;18(35):24173–24181. doi: 10.1021/acsnano.4c05560
[37] Leitis A, Tseng ML, John-Herpin A, et al. Wafer-scale functional metasurfaces for mid-infrared photonics and biosensing. Adv Mater. 2021;33(43):2102232. doi: 10.1002/adma.202102232
[38] Huang Z-T, Chang C-Y, Chen K-P, et al. Tunable lasing direction in one-dimensional suspended high-contrast grating using bound states in the continuum. Adv Photon. 2022;4(6):066004. doi: 10.1117/1.AP.4.6.066004
[39] Shen SJ, Lee B-R, Peng YC, et al. Dielectric high-Q metasurfaces for surface-enhanced deep-UV absorption and chiral photonics. ACS Photonics. 2025;12(6):2955–2964. doi: 10.1021/acsphotonics.4c01960
[40] Palik ED, editor. Handbook of optical constants of solids. Vol. 3. Orlando: Academic press; 1998.
[41] Rakić AD, Djurišić AB, Elazar JM, et al. Optical properties of metallic films for vertical-cavity optoelectronic devices. Appl Opt. 1998;37(22):5271–5283. doi: 10.1364/AO.37.005271
[42] Taubert R, Hentschel M, Kästel J, et al. Classical analog of electromagnetically induced absorption in plasmonics. Nano Lett. 2012;12(3):1367–1371. doi: 10.1021/nl2039748
[43] Li Z, Butun S, Aydin K. Ultranarrow band absorbers based on surface lattice resonances in nanostructured metal surfaces. ACS Nano. 2014;8(8):8242–8248. doi: 10.1021/nn502617t